Enhanced Tracking of DC-DC Buck Converter Systems Using Reduced-Order Extended State Observer-Based Model Predictive Control

Bozhao Wang [ORCID], Shengquan Li*[ORCID], Shiqi Kan[ORCID], Juan Li[ORCID]

College of Electrical, Energy and Power Engineering, Yangzhou University, 225127 Yangzhou, China

* Correspondence: Shengquan Li (sqli@yzu.edu.cn)

Citation: B. Z. Wang, S. Q. Li, S. Q. Kan, and J. Li, "Enhanced tracking of DC-DC buck converter systems using reduced-order extended state observer-based model predictive control," *J. Intell Syst. Control*, vol. 2, no. 3, pp. 143–152, 2023. https://doi.org/10.56578/jisc020303.

Abstract: In this study, the challenges of load variations, input voltage fluctuations, and reference voltage deviations for a DC-DC buck converter system are addressed. A composite voltage controller, founded on a model predictive control (MPC) integrated with a reduced-order state observer (RESO), is introduced to ameliorate the tracking performances of such converters. Disturbances, both matched and mismatched, are conceptualized as total disturbances within an innovatively proposed error tracking model. Subsequently, a RESO is meticulously developed to estimate and attenuate these disturbances. In parallel, an MPC is crafted to ensure enhanced system robustness and superior steady-state performances. Comparative simulations indicate that this innovative composite controller exhibits a rapid settling time and smoother response curve compared to traditional MPC. Furthermore, it is observed that when exposed to disturbances, the proposed methodology demonstrates heightened disturbance rejection capabilities, accelerated voltage tracking, and improved steady-state performance.

Keywords: DC-DC conversion; Buck converter; MPC; RESO; Disturbance rejection

1 Introduction

Amid the escalating demand for DC power supply and DC grids, DC-DC converters have been extensively studied and employed across various DC circuits, encompassing renewable energy sources (RESs), energy storage systems (ESSs), and interfacing devices. A pivotal role in these applications is played by DC-DC converters, primarily serving as a nexus between the DC bus and DC load, each having diverse voltage or power specifications. Of all the DC-DC converters, the DC-DC buck converter stands as one of the most fundamental and emblematic. However, it has been observed that such converters inevitably encounter both internal and external disturbances, collectively termed as total disturbances [1]. These disturbances have been identified to comprise uncertainties in power generation equipment, electromagnetic noise, and variations in load [1]. Moreover, challenges posed by input variations have been perceived to be more intricate compared to load changes [1]. Such complications are believed to escalate risks of power loss and potential equipment damage [2].

For buck converters, achieving optimal dynamic and static performance in the face of these disturbances and varying operational conditions has been deemed imperative. Previous research findings have indicated the potential benefits of refining circuit topology or control strategy to bolster the DC converter's anti-disturbance rejection capability and voltage tracking performance [3]. In numerous practical scenarios, the introduction of cutting-edge control strategies has been recognized as a straightforward and viable solution [4]. Yet, achieving desired control outcomes has been achieved by overhauling existing DC converter circuits, often accompanied by significant costs and extended developmental cycles [4]. A myriad of controllers, including proportional-integral (PI) control, model predictive control (MPC), sliding mode control (SMC), fuzzy control, and active disturbance rejection control (ADRC), have been explored for electrical power converters [5–7]. A notable approach, the fuzzy SMC, was designed to supplant the traditional PI controller, primarily to curtail chattering phenomena and heighten robustness [5]. Furthermore, an enhanced linear ADRC was suggested to address the pronounced degradation of power quality during microgrid disturbances [6]. Thus, a comprehensive analysis of advanced control strategies

is believed to facilitate effortless parameter tuning and promote superior dynamic and static performance of power converter systems.

Renowned for its adeptness in managing multiple-input-multiple-output (MIMO) systems with diverse constraints, MPC has been extensively employed, particularly within the power electronics realm, owing to its robustness and commendable steady-state performance [7]. Typically, the core components of MPC encompass a predictive model, a cost function designated for weight tuning, and a receding horizon for periodic amendments [8]. A recent study proposed an MPC-based scheme tailored for a dual active bridge DC-DC converter to elevate its dynamic performance while adhering to current stress limitations [8]. An intriguing revelation in this field has been the fractional order of real-world inductance and capacitance, implying that the current and voltage derivative relations for these components deviate from the integer order [9]. Nevertheless, the intrinsic ability of MPC to adjust its horizon periodically has been postulated to exhibit commendable resilience against non-linearities and system uncertainties [10]. Consequently, MPC emerges as a promising alternative control technique for the DC-DC buck converter, aiming to mitigate external disturbances and model uncertainties.

Historical models of the DC-DC buck converter were conceptualized with capacitance voltage and inductance current as primary states. These models were often accompanied by both matched and mismatched disturbances [11]. The emergence of mismatched disturbances is suspected to potentially prolong convergence time, suggesting that disturbance capabilities might be compromised by these mismatched disturbances [11]. Traditional physical testing systems have found the differentiation of output voltage challenging. However, observer-based soft sensing technology was identified as an optimal solution in practical engineering contexts [12]. Consequently, an output error tracking model has been proposed to address these challenges, given its capability to reclassify mismatched disturbance as matched disturbance [13].

Furthermore, observer-based control methods such as extended state observer (ESO), disturbance observer (DO), and generalized proportional-integral observer (GPIO) have been acknowledged as efficacious methodologies for disturbance estimation and compensation, rooted in the inner model theory. Predominantly, these control techniques are observed to mitigate both internal and external disturbances through a feed-forward channel in real-world control systems [14]. For instance, a robust DO-based adaptive SMC strategy was conceptualized for humanoid support robots, aiming to stabilize tracking errors within a stipulated timeframe [14]. Similarly, an ESO focused on the state model was developed to address both external and internal disturbances and uncertainties [15]. In another endeavor, a GPIO-aligned super-twisting SMC was crafted to enhance the tracking precision of the permanent magnet synchronous motor (PMSM) speed regulation system [16]. However, potential challenges for these observer methods, such as lagging observer convergence rates or overwhelming observer computations when paired with MPC, have been highlighted.

In the context of DC-DC buck converters, the disturbances - both internal and external - have been meticulously examined and subsequently categorized as total disturbances. The primary impetus behind this study revolves around the development of an optimized voltage tracking strategy for DC-DC buck converters, especially in light of input fluctuations and load variations. Consequently, an RESO integrated with a model predictive controller has been proposed, aiming to expedite the voltage tracking process of the DC-DC buck converter. The adoption of the MPC approach facilitates a cohesive design methodology, ensuring adherence to physical constraints while maintaining optimal steady and dynamic performances. Furthermore, a discrete average model has been introduced to both design and predict the continuous conduction mode (CCM), solidifying system stability and bolstering its anti-disturbance capabilities.

The notable contributions of this research can be distilled into the following points:

• A novel model has been formulated that amalgamates both matched and mismatched disturbances under the umbrella of total disturbances. It was observed that the rate of convergence remained uninhibited by the presence of mismatched disturbances.

• The implementation of RESO showcased an enhanced anti-disturbance capacity, particularly in response to deviations in input voltage and load resistance, demonstrating a more rapid convergence compared to the conventional ESO.

The structure of this article is organized systematically. In Section II, the innovative state-space system model, focused on the tracking error of the buck converter, is elucidated. The underlying principles of the proposed RESO-MPC are explored in depth in Section III. Performance assessments, grounded in simulation cases, are presented in Section IV. The article culminates in Section V, drawing conclusions from the research undertaken.

2 Buck Converter Modeling

Within the context of CCM, the average state equation of the buck converter has been introduced, as depicted in Figure 1. Subsequently, an error-tracking state equation was derived based on this average state equation.

As illustrated in Figure 1, the circuit topology of the buck converter encompasses several key components: A MOSFET (Metal-Oxide-Semiconductor Field-Effect Transistor) switch denoted as S, a diode labeled D, an inductance

L with its associated resistance r_L and a capacitance C. Here Vin and R are representative of the input voltage and the load's equivalent resistance, respectively.
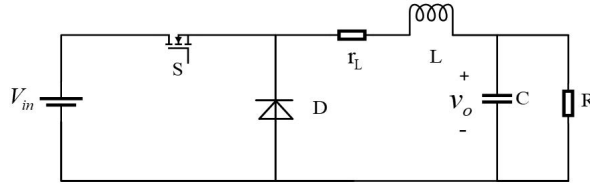

Figure 1. Circuit topology of the buck converter

Drawing from Kirchhoff's current and voltage theorems, the average state equation of the buck converter in CCM can be represented as:

$$\begin{cases} i_L = \frac{\mu V_{in}}{L} - \frac{v_o}{L} \\ \dot{v}_o = \frac{i_L}{C} - \frac{v_o}{CR} \end{cases} \tag{1}$$

where, i_L and v_o denote the inductor current and capacitor voltage, in that order. The duty ratio is defined by μ.

Output error tracking states are subsequently defined as:

$$\begin{cases} x_1 = v_o - V_r \\ x_2 = \dot{x}_1 \end{cases} \tag{2}$$

where, x_1 captures the variance between the output voltage v_o and the reference output voltage V_r, whereas x_2 is indicative of the differentiation of x_1, effectively representing the differentiation of output voltage v_o.

Building upon Eq. (1), the output voltage error tracking state equation can be formulated as:

$$\begin{cases} \dot{x}_1 = x_2 \\ \dot{x}_2 = \ddot{x}_1 = \frac{\mu V_{in} - v_r}{LC} - \frac{x_1}{LC} - \frac{x_2}{RC} \end{cases} \tag{3}$$

Given that the real input voltage and resistive load may diverge from their nominal counterparts, the discrepancies between real and nominal values can be perceived as disturbances. This insight allows for the reconstruction of the error tracking state model, as seen in Eq. (4):

$$\begin{cases} \dot{x}_1 = x_2 \\ \dot{x}_2 = \ddot{x}_1 = \frac{\mu V_{in0} - v_r}{LC} - \frac{x_1}{LC} - \frac{x_2}{R_0 C} + d(t) \end{cases} \tag{4}$$

where, V_{in0} and R_0 are the nominal values of V_{in} and R, respectively. The encompassing disturbances are described by $d(t) = \frac{\mu}{LC}(V_{in} - V_{in0}) + \dot{x}_1(\frac{1}{R_0 C} - \frac{1}{RC})$. It should be noted that other forms of disturbances exhibit a linear dependence on R and V_{in}, suggesting their equivalence to the total disturbances.

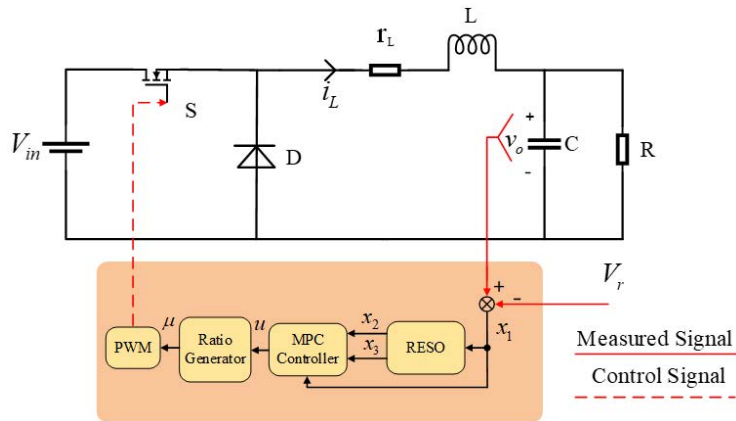## 3 The RESO-MPC Approach: Conceptualization and Design

Figure 2. Structural blueprint of the RESO-MPC strategy

In this section, the architectural design of the RESO for state and disturbance estimation is elucidated. Parallelly, the fundamentals of MPC are laid down, affirming its role as the primary controller.

As demonstrated in Figure 2, the intricate design of the RESO-MPC architecture emerges. It can be discerned that the RESO is formulated primarily for estimating state variables and the collective disturbances. Utilizing the output voltage data, alongside the RESO-estimated values, the MPC is then assembled. Culminating this process, a PWM signal is sculpted based on the controller's output, steering the buck converter's switch.

3.1 The Blueprint of the RESO

Considering the intrinsic challenges in measuring the state variable x_2 using conventional physical sensors, observer-based soft sensor techniques are employed for x_2 estimation. This method offers the luxury of concurrently estimating both x_2 and the aggregate disturbances, denoted as d. Viewing the total disturbances as a novel state variable for ESO, the state space equation can be expanded as:

$$\begin{cases} \dot{x}_1 = x_2 \\ \dot{x}_2 = \ddot{x}_1 = \frac{\mu V_{in0} - v_r}{LC} - \frac{x_1}{LC} - \frac{x_2}{R_0 C} + x_3 \\ \dot{x}_3 = \dot{d} \end{cases} \tag{5}$$

From this, an ESO stemming from Eq. (5) is architectured as:

$$\begin{cases} \dot{z}_1 = z_2 - l_1 (z_1 - x_1) \\ \dot{z}_2 = \frac{\mu V_{in0} - v_r}{LC} - \frac{x_1}{LC} - \frac{1}{R_0 C} z_2 + z_3 - l_2 (z_2 - x_1) \\ \dot{z}_3 = -l_3 (z_2 + \beta_1 z_1) \end{cases} \tag{6}$$

where, l_1, l_2, l_3 are recognized as the observer gains. The parameters z_1, z_2, z_3 serve as the estimated values for x_1, x_2, x_3, respectively. The convergence rate, dictated by the observer gain, is intriguing: a more substantial observer gain accelerates the ESO convergence rate. However, caution is mandated, as a surge in gain might induce oscillations. Thus, ADRC parameter selection becomes pivotal. Given that the ESO foundation is rooted in state feedback, the value of the state variable becomes essential. A noteworthy observation is the tight relationship between the estimation discrepancies of z_2, z_3 and x_2, x_3 with the precision of estimated values of z_1 and x_1. Moreover, z_1 is designed to shadow x_1, and the latter can be measured directly via a voltage sensor. Consequently, the RESO, backed by the measured value x_1, can be garnered at a rate outpacing the ESO. The RESO is thus expressed as:

$$\begin{cases} \dot{z}_2 = \frac{\mu V_{in0} - v_r}{LC} - \frac{x_1}{LC} - \frac{1}{R_0 C} (z_2 + \beta_1 x_1) + z_3 + \beta_2 x_1 - \beta_1 (z_2 + \beta_1 x_1), \\ \dot{z}_3 = -\beta_2 (z_2 + \beta_1 x_1), \\ \hat{x}_2 = z_2 + \beta_1 x_1, \hat{x}_3 = z_3 + \beta_2 x_1 \end{cases} \tag{7}$$

where, β_1, β_2 signify the RESO gains. Outputs from RESO, $\hat{x}_2, \hat{x}_3$ reflect the estimated values.

To dissect the disturbance sensitivity innate to the proposed RESO, transform functions rooted in Eq. (7) are computed, resulting in:

$$\frac{\Delta \hat{x}_2}{\Delta x_1} = \frac{\Delta z_2 + \beta_1 \Delta x_1}{\Delta x_1} = \frac{dz_2}{dt} \frac{x_1}{z_2} + \beta_1 \simeq \left(\frac{\frac{\mu V_{in0} - v_r}{LC} - \frac{x_1}{LC} + z_3 + \beta_2 x_1}{z_2 + \beta_1 x_1} - \frac{1}{R_0 C} - \beta_1 \right) \frac{x_1}{z_2} + \beta_1 \tag{8}$$

$$\frac{\Delta \hat{x}_3}{\Delta x_1} = \frac{\Delta z_3 + \beta_3 \Delta x_1}{\Delta x_1} = \frac{dz_3}{dt} \frac{x_1}{z_3} + \beta_2 = -\beta_2 \frac{x_1}{z_3} + \beta_2 \tag{9}$$

From a synthesis of Eqs. (8)-(9), a remarkable observation can be made: a disturbance impact on x_1 precipitates a swift surge in $\hat{x}_2$ and $\hat{x}_3$. Additionally, a more pronounced disturbance effect on x_1 magnifies the volatility in the ranges of $\hat{x}_2$ and $\hat{x}_3$.

3.2 MPC: Design and Framework

In the context of this study, x_1 is selected as the output variable, from which the state space equation is derived as:

$$\begin{aligned} \dot{X} &= A_c X + B_{cu} u + B_{cd} d \\ y &= C_c X \end{aligned} \tag{10}$$

where, $X = \begin{bmatrix} x_1 & x_2 \end{bmatrix}^T$, $u = \frac{\mu V_{in0} - v_r}{LC}$, $d = \frac{1}{LC}(V_{in} - V_{in0}) + \dot{x}_1(\frac{1}{R_0C} - \frac{1}{RC})$, $A_c = \begin{bmatrix} 0 & 1 \\ -\frac{1}{LC} & -\frac{1}{R_0C} \end{bmatrix}$, $B_{cu} = \begin{bmatrix} 0 & 1 \end{bmatrix}^T$, $B_{cd} = \begin{bmatrix} 0 & 1 \end{bmatrix}^T$, $C_c = \begin{bmatrix} 1 & 0 \end{bmatrix}$. The continuous time state space represented in Eq. (4) is transformed into the discrete time state space equation as illustrated in Eq. (11), achieved using the Euler approximation depicted in Eq. (12):

$$X(k+1) = A_dX(k) + B_{du}u(k) + B_{dd}d(k)$$
$$y(k) = C_dX(k) \tag{11}$$

where, $A_d = I + A_cT_s$, $B_{du} = B_{cu}T_s$, $B_{dd} = B_{cd}T_s$, $C_d = C_c$. The matrix symbol I and time notation T_s are unit matrix and sampling time. The Euler approximation equation developed in the paper can be shown as follows:

$$\frac{dx(t)}{dt} = \frac{x(k+1) - x(k)}{T_s} \tag{12}$$

Transitioning from the discrete state space equation, Eq. (11) is adapted into its incremental form by invoking the incremental equation, Eq. (14), resulting in Eq. (13):

$$\Delta X(k+1) = A_d\Delta X(k) + B_{du}\Delta u(k) + B_{dd}\Delta d(k)$$
$$y(k) = C_d\Delta X(k) + y(k-1) \tag{13}$$

$$\Delta X(k+1) = X(k+1) - X(k) \tag{14}$$

where, $\Delta d(k) = \hat{x}_3(k) - \hat{x}_3(k-1)$ is the defined parameter. Consequently, the augmented state space equation emerges as:

$$\bar{X}(k_i + 1 \mid k_i) = A\bar{X}(k_i) + B\Delta u(k_i) + B_d\Delta d(k_i)$$
$$y(k_i + 1 \mid k_i) = C\bar{X}(k_i + 1 \mid k_i) \tag{15}$$

where, $\bar{X}(k_i) = \begin{bmatrix} \Delta X(k) \\ y(k) \end{bmatrix}$ denotes augmented state vector, $\bar{X}(k_i + 1 | k_i)$ and $y(k_i + 1 | k_i)$ denote the prediction of the state quantity and system output at $k_i + 1$ steps at moment k_i, respectively. The output matrix Y, as following Eq. (16), can be obtained after a series of derivations of future state quantities and output predictions, by defining $\Delta u(k+i) = 0, i = N_c, N_c + 1, N_c + 2, ..., N_p - 1$ and $\Delta d(k+i) = 0, i = 1, 2, ..., N_p - 1$.

$$Y = F\bar{X}(k_i) + \Phi\Delta U + D\Delta d(k_i) \tag{16}$$

where,

$$F = \begin{bmatrix} CA \\ CA^2 \\ \vdots \\ CA^{N_p} \end{bmatrix},$$

$$\Phi = \begin{bmatrix} CB & 0 & 0 & 0 \\ CAB & CB & 0 & 0 \\ ... & ... & ... & CA^{N_p - N_c - 1}B \\ CA^{N_p - 1}B & CA^{N_p - 2}B & ... & CA^{N_p - N_c}B \end{bmatrix},$$

$$D = \begin{bmatrix} CB_d & CAB_d & ... & CA^{N_p - 1}B_d \end{bmatrix},$$

$$Y = \begin{bmatrix} y(k_i + 1 | k_i) & y(k_i + 2 | k_i) & ... & y(k_i + N_p | k_i) \end{bmatrix}^T,$$

$$\Delta U = \begin{bmatrix} \Delta u(k_i) & \Delta u(k_i + 1) & ... & \Delta u(k_i + N_c - 1) \end{bmatrix}^T.$$

The parameter matrixes are defined as $A = \begin{bmatrix} A_d & 0_m^T \\ C_dA_d & 1 \end{bmatrix}$, $B = \begin{bmatrix} B_{du} \\ C_dB_{du} \end{bmatrix}$, $B_d = \begin{bmatrix} B_{dd} \\ C_dB_{dd} \end{bmatrix}$, $C = \begin{bmatrix} 0_m & 1 \end{bmatrix}$. The cost function can be defined as follows:

$$J = (R_s - Y)^T(R_s - Y) + \Delta U^T\bar{R}\Delta U \tag{17}$$

where, $R_s^T = \underbrace{\begin{bmatrix} 1 & 1 & ..... & 1 \end{bmatrix}}_{N_p} r(k_i)$ denotes the reference of matrix Y. The notation $\bar{R} = r_wI_{N_c \times N_c}$ is the weighting coefficients of the cost function. The coefficients r_w and $I_{N_c \times N_c}$ mean feedback factor and the unit matrix of $N_c \times N_c$

order. Considering the output as the difference between the output voltage and its actual expectation, the expectation should converge to 0, which means $r(k_i) = 0$. The partial derivative of Eq. (16) should be equal to 0, so the solution can be obtained as follows:

$$\Delta U = \left(\Phi^T \Phi + \bar{R} \right)^{-1} \Phi^T \left(-Fx(k_i) - D\Delta d(k_i) \right) \tag{18}$$

Given that the MPC necessitates receding in the time domain and recalculates per sample, the control variable for each output emerges as:

$$\Delta u = \underbrace{\begin{bmatrix} 1 & 0 & \cdots & 0 \end{bmatrix}}_{N_c} \Delta U \tag{19}$$

However, due to the modulation wave's width constraints u, on the control law μ, a constraint is deduced, encapsulated in Eq. (20):

$$\mu = \frac{uLC + v_r}{V_{in0}}, \mu \in (0, 1) \tag{20}$$

This constraint on u is further depicted in:

$$u \in \left(\frac{-v_r}{LC}, \frac{V_{in0} - v_r}{LC} \right) \tag{21}$$

Consequently, the control law $u(t)$ is articulated as:

$$u(t) = \begin{cases} -\frac{v_r}{LC}, & \Delta u(t) + u(t-1) \leq -\frac{v_r}{LC} \\ \Delta u(t) + u(t-1), & -\frac{v_r}{LC} < \Delta u(t) + u(t-1) < \frac{V_{in0} - v_r}{LC} \\ \frac{V_{in0} - v_r}{LC}, & \Delta u(t) + u(t-1) \geq \frac{V_{in0} - v_r}{LC} \end{cases} \tag{22}$$

4 Convergence and Stability Analysis

This section delves into the convergence properties of RESO and the stability characteristics of the closed-loop system, explored under a specific set of assumptions and lemmata.

4.1 Convergence Attributes of ESO

Given the potential abrupt surges in total disturbance from the input voltage and load resistance, coupled with the error tracking state equation, Assumption 1 and Lemma 4.1 are posited:

Assumption 1. For the above DC-DC buck system (4), The total disturbances $d(t)$ can be supposed to be bounded and satisfied $\lim_{t \to 0} \dot{d}(t) = 0$.

Lemma 4.1. [17] Considering that a nonlinear system $\dot{x} = F(x, w)$ is satisfied input-to-state stable (ISS), the state variable condition $\lim_{t \to 0} x(t) = 0$ is satisfied, if the input condition $\lim_{t \to 0} w(t) = 0$ is satisfied.

Proof. Errors arising between the observer estimated values and the actual system state variables can be expressed as $\xi_2 = \hat{x}_2 - x_2, \xi_3 = \hat{x}_3 - x_3$, leading to the subsequent relation expressed in Eq. (23):

$$\begin{cases} \dot{\xi}_2 = -\left(\beta_1 + \frac{1}{R_0 C} \right) \xi_2 + \xi_3 \\ \dot{\xi}_3 = -\beta_2 \xi_2 - \dot{d} \\ \xi_2 = \hat{x}_2 - x_2, \xi_3 = \hat{x}_3 - x_3 \end{cases} \tag{23}$$

where, d encapsulates the total disturbances. The integration of observer errors, portrayed in Eq. (24), can be executed as:

$$\dot{\xi} = A_{ESO} \xi + B_{ESO} \dot{d} \tag{24}$$

where, $\xi = [\xi_2, \xi_3]^T$, $A_{ESO} = \begin{bmatrix} -(\beta_1 + \frac{1}{R_0 C}) & 1 \\ -\beta_2 & 0 \end{bmatrix}$, $B_{ESO} = [ll0 - 1]$. Then, the eigenvalues of system matrix A_{ESO} can be calculated from characteristic equation:

$$\det(\lambda I - A_{ESO}) = \lambda^2 + \left(\beta_1 + \frac{1}{R_0 C} \right) \lambda + \beta_2 = 0 \tag{25}$$

where, in alignment with prior definitions, $\beta_1 + \frac{1}{R_0 C} > 0, \beta_2 > 0$ represents the eigenvalue. It becomes evident that the system pole resides within the left half plane. Thus, in alignment with Lemma 4.1, and ensuring that the disturbance under consideration conforms to Assumption 1, it is inferred that the observer exhibits convergence.

4.2 Stability Analysis for Closed-loop

To demonstrate the stability of closed-loop, Lemma 4.2 is necessary to introduce based on Lyapunov function.

Lemma 4.2. [18] Consider a closed-loop system under MPC scheme asymptotically stable. If there exists Lyapunov function $V(x)$ satisfies the following equation and inequation, then the closed-loop system is asymptotically stable:

1) $V(X(k)) \geq 0$ for all x and $V(0) = 0$,

2) $\Delta V(x) = V(f(x)) - V(x)$ for all x.

Proof. Substituting Eq. (16) in Eq. (17) and sort it out:

$$\Delta u = \underbrace{\begin{bmatrix} 1 & 0 & \cdots & 0 \end{bmatrix}}_{N_c} \left(\Phi^T \Phi + \bar{R}\right)^{-1} \Phi^T \left(-Fx(k_i) - D\Delta d(k_i)\right)$$
$$= -K_{MPC} x(k_i) - K_d \Delta d(k_i) \tag{26}$$

where, K_{MPC} and K_d are state feedback control gain using MPC and feedback control gain related to $\Delta d(k_i)$ respectively. Then, by substituting the Eq. (26) into Eq. (15), the closed-loop state-space equation of the system can be obtained as follows:

$$\bar{X}(k_i + 1 \mid k_i) = (A - BK_{MPC}) \bar{X}(k_i) + (B_d - BK_d) \Delta d(k_i) \tag{27}$$

The Lyapunov function can be given as following Eqs. (27)-(28), to introduce the analysis the stability of the closed-loop system:

$$V(x(k)) = x^2(k) \tag{28}$$

$$\Delta V(\bar{X}(k)) = \bar{X}^2(k + 1 \mid k) - \bar{X}^2(k)$$
$$= \left(B_{close} \bar{X}(k) + B_{dclose} \Delta d(k)\right)^2 - (\bar{X}(k))^2 \tag{29}$$
$$\simeq \left(I - B_{close}^2\right) (\bar{X}(k))^2 + B_{dclose}^2 (\Delta d(k))^2$$

where, $B_{close} = (A - BK_{MPC})$. In addition, matrix $B_{dclose} = (B_d - BK_d)$ are control matrixes and disturbance matrixes of the closed-loop system. If the disturbance satisfies Assumption 4.1, the following inequality can be satisfied:

$$-\left(I - B_{close}^2\right) \bar{X}^2(k) + B_{dclose}^2 (\Delta d(k))^2 \leq 0 \tag{30}$$

Obviously, the following inequation (31) can be deduced:

$$\Delta V(\bar{X}(k)) \leq -\left(I - B_{close}^2\right) (\bar{X}(k))^2 + B_{dclose}^2 (\Delta d(k))^2 \tag{31}$$

Thus,

$$\Delta V(\bar{X}(k)) \leq 0, \forall \bar{X}^2(k) \geq \left(I - B_{close}^2\right)^2 B_{dclose}^2 (\Delta d(k))^2 \tag{32}$$

As a result, by substituting the value of BMPC and Bd, inequation (32) means that the closed-loop system (26) is stable with respect to bounded $\Delta d(k)$.

## 5 Simulation Results and Analysis

Within this section, the parameters pertaining to the DC-DC buck converter, as well as the resultant simulation data, are detailed. Emphasis is placed on discerning the robustness and steady-state efficacy of the proposed RESO-MPC scheme through comparative simulations against the conventional MPC. For the purpose of these simulations, the buck converter was operated in a CCM to ensure its alignment with the desired model. MATLAB/Simulink was employed for these simulations, with initial conditions being configured to match desired input voltage levels. Essential component parameters of the DC-DC buck converter are delineated in Table 1.

Figures 3, 4, and 5 illustrate the performance metrics of the RESO-MPC, ESO-MPC, and the conventional MPC in scenarios encompassing variations in input voltage, output load, and reference output voltage, respectively. Specifically:

• Figure 3 captures the scenario wherein the input voltage undergoes a decline from 10 V to 9 V, subsequently surging to 10.5 V.

• Figure 4 documents the condition wherein resistance undergoes a significant reduction, decreasing from 300 Ω to 150 Ω.

• Figure 5 chronicles the event where the reference descends from 6 V to 8 V, followed by an elevation to 5 V.

Table 1. Parameters of the DC-DC buck converter

Parameters	Symbol	Value
Input voltage	E	10 V
Desire input voltage	V_r	5 V
Inductance	L	4.7mH
Capacitance	C	4.7μF
Load resistance	R	300Ω
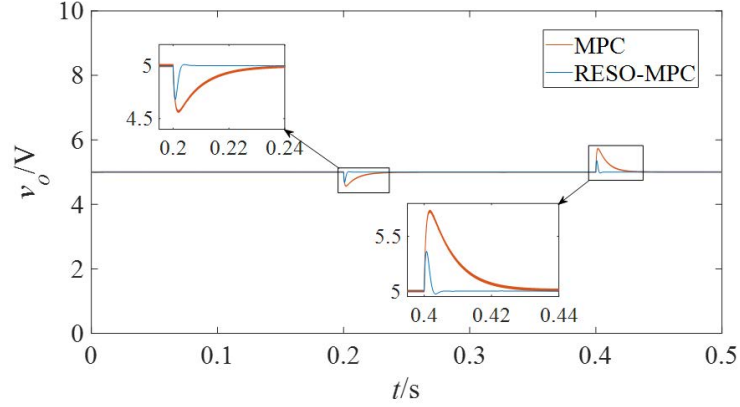
Figure 3. Comparative response dynamics under RESO-MPC and MPC during input voltage variation
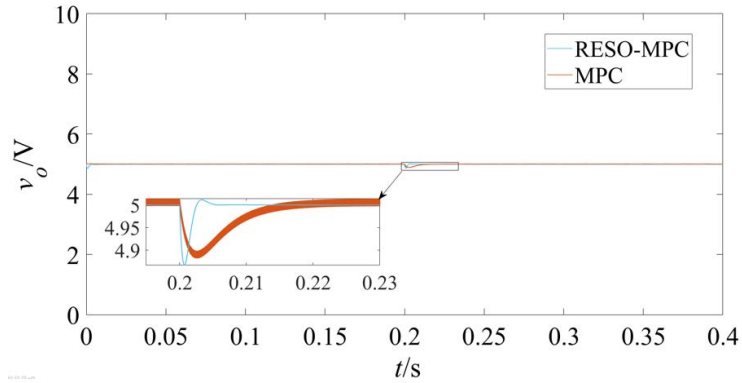
Figure 4. Comparative response dynamics under RESO-MPC and MPC during load resistance adjustments
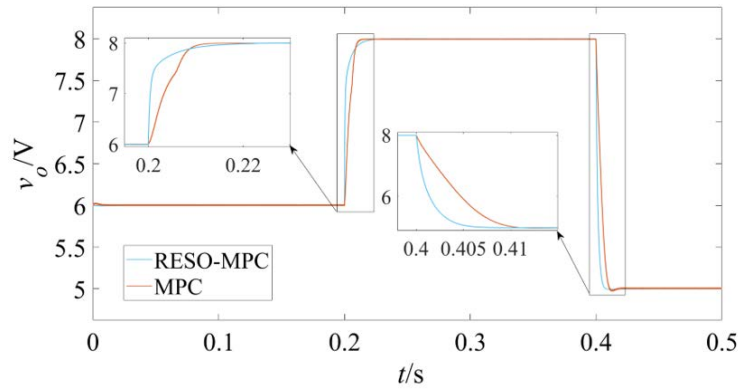
Figure 5. Comparative response dynamics under RESO-MPC and MPC with variations in reference output

Drawing from Figures 3 and 4, it is observed that the settling time for output voltage governed by the RESO-MPC controller is accelerated by margins of 0.03s and 0.01s compared to the MPC controller, during input voltage and load

resistance alterations, respectively. Further insights from Figure 5 indicate that during transitions of output voltage from 6 V to 8 V and from 8 V to 5 V, the RESO-MPC-controlled system demonstrated a swifter settling time by 0.01s and 0.005s, respectively, compared to its MPC counterpart. Additionally, a discernable reduction in response curve variance of the output voltage, amounting to 0.12 V and 0.8 V, is noted under the RESO-MPC controller, as contrasted with the MPC controller during input voltage fluctuations.

The analyzed simulation outcomes underscore the superior anti-disturbance and dynamic performance inherent to the RESO-MPC controller relative to the traditional MPC. Figures 3 and 4 corroborate the enhanced disturbance rejection capability of the RESO-MPC controller in the presence of external perturbations. Figure 5 further accentuates the proficiency of the RESO-MPC controller in swiftly achieving target values devoid of overshoots, while the conventional MPC exhibited a more protracted approach with noticeable overshoots. In essence, for DC-DC buck converters, the RESO-MPC controller emerges as a paradigm demonstrating commendable steady-state and dynamic performance coupled with an elevated anti-disturbance capacity.

6 Conclusions

The disturbance attenuation challenge within the context of the input and output of the DC-DC buck converter has been meticulously explored. An RESO was meticulously designed to estimate both state and disturbance variables. Convergence and stability were rigorously assessed using input-to-state stability criteria combined with Lyapunov theory. Through simulation, the efficacy of the presented control strategy was confirmed.

The following salient observations emerged from the simulation and experimental results:

• Firstly, the RESO exhibited an enhanced capability for tracking and resisting disturbances stemming from alterations in input voltage and load resistance.

• Secondly, the introduced RESO-MPC controller demonstrated superior dynamic performance in comparison to traditional MPC.

These findings corroborate the premise that a buck converter governed by a RESO-MPC controller can sustain high-quality outputs and efficiently counteract disturbances, even in the presence of sub-optimal circuit conditions.

The application of the proposed RESO-MPC strategy to converters boasting intricate topologies and diverse functionalities warrants further exploration, particularly in navigating multifaceted disturbances. Concurrently, further refinements and computational optimizations remain imperative for enhancing the MPC's performance.

Future research endeavors may extend the present study by examining the applicability and robustness of the RESO-MPC strategy across a wider array of converters and operational scenarios, thereby broadening its scope and potential utility.

Funding

Data Availability

The data used to support the findings of this study are available from the corresponding author upon request.

Conflicts of Interest

The authors declare that they have no conflicts of interest.

References

[1] S. N. Mirebrahimi, F. Merrikh-Bayat, and A. Taheri, "Voltage-mode robust controller design for DC-DC boost converter at the presence of wide load and input voltage variations based on finite-state-machine model," *IET Power Electron.*, vol. 11, no. 5, pp. 866–875, 2018. http://doi.org/10.1049/iet-pel.2017.0136

[2] O. D. Montoya, W. Gil-González, S. Riffo, C. Restrepo, and C. González-Castaño, "A sensorless inverse optimal control plus integral action to regulate the output voltage in a boost converter supplying an unknown DC load," *IEEE Access*, vol. 11, pp. 49 833–49 845, 2023. http://doi.org/10.1109/ACCESS.2023.3277750

[3] B. Long, D. Shen, T. Cao, J. Rodriguez, J. M. Guerrero, K. Chong, and Y. Teng, "Passivity-based partial sequential model predictive control of T-type grid-connected converters with dynamic damping injection," *IEEE Trans. Power Electron.*, vol. 38, no. 7, pp. 8262–8281, 2023. https://doi.org/10.1109/TPEL.2023.3266588

[4] N. Surulivel, D. Debnath, and C. Chakraborty, "Novel bidirectional four-port DC–DC converter suitable for bipolar DC solar household integration," *IEEE Trans. Power Electron.*, vol. 38, no. 7, pp. 9033–9045, 2023. http://doi.org/10.1109/TPEL.2023.3249339

[5] Y. Rekha, V. Jamuna, and I. W. Christopher, "Cascaded inner loop fuzzy SMC for DC-DC boost converter," *J. Circuits Syst. Comput.*, p. 2350269, 2023. http://doi.org/10.1142/s0218126623502699

[6] Y. Wang, L. Tao, P. Wang, X. Ma, P. Cheng, and D. Zhao, "Improved linear ADRC for hybrid energy storage microgrid output-side converter," *IEEE Trans. Ind. Electron.*, vol. 69, no. 9, pp. 9111–9120, 2022. http://doi.org/10.1109/TIE.2021.3116573

[7] L. F. D. Pereira, E. A. Batista, J. O. P. Pinto, B. R. Upadhyaya, J. W. Hines, and J. B. Coble, "Model predictive control for sodium fast reactors based on laguerre functions and FPGA-in-the-loop environment," *Nucl. Eng. Des.*, vol. 400, p. 112041, 2022. http://doi.org/10.1016/j.nucengdes.2022.112041

[8] S. M. Akbar, A. Hasan, A. J. Watson, and P. Wheeler, "Model predictive control with triple phase shift modulation for a dual active bridge DC-DC converter," *IEEE Access*, vol. 9, pp. 98 603–98 614, 2021. http://doi.org/10.1109/access.2021.3095553

[9] S. L. Li, P. K. Li, Z. Zheng, and T. Huang, "Fractional order sliding mode control for circulating current suppressing of MMC," *Electr. Eng.*, 2023. http://doi.org/10.1007/s00202-023-01902-7

[10] U. Rosolia, D. C. Guastella, G. Muscato, and F. Borrelli, "Model predictive control in partially observable multi-modal discrete environments," *IEEE Control Syst. Lett.*, vol. 7, pp. 2161–2166, 2023. http://doi.org/10.1109/LCSYS.2023.3284807

[11] J. Li, S. W. Wang, L. Y. Zhang, and S. Q. Li, "Nonlinear cascade sliding mode control based on extended state observer method for a DC-DC buck converter: Design and hardware experimentation," *Proc. Inst. Mech. Eng. I-J. Syst. Control Eng.*, vol. 237, no. 4, pp. 608–621, 2023. http://doi.org/10.1177/09596518221133472

[12] O. Babayomi and Z. B. Zhang, "Model-free predictive control of power converters with cascade-parallel extended state observers," *IEEE Trans. Ind. Electron.*, vol. 70, no. 10, pp. 10 215–10 226, 2023. http://doi.org/10.1109/tie.2022.3217609

[13] S. Wang, L. Juan, L. Zhang, and S. Li, "Cascade sliding mode control based on extended state observer method for a DC-DC buck converter," in *2021 40th Chinese Control Conference (CCC), Shanghai, China*, 2021, pp. 2366–2371. http://doi.org/10.23919/CCC52363.2021.9549771

[14] X. J. Su, F. D. Qing, H. B. Chang, and S. Y. Wang, "Trajectory tracking control of human support robots via adaptive sliding-mode approach," *IEEE Trans. Cybern.*, pp. 1–8, 2023. http://doi.org/10.1109/tcyb.2023.3253171

[15] X. Liu, L. Qiu, W. Wu, J. Ma, D. Wang, Z. Peng, and Y. Fang, "Finite-time ESO-based cascade-free FCS-MPC for NNPC converter," *Int. J. Electr. Power Energy Syst.*, vol. 148, p. 108939, 2023. http://doi.org/10.1016/j.ijepes.2022.108939

[16] Q. Hou and S. Ding, "GPIO based super-twisting sliding mode control for PMSM," *IEEE Trans. Circuits Syst. II Express Briefs*, vol. 68, no. 2, pp. 747–751, 2021. http://doi.org/10.1109/TCSII.2020.3008188

[17] J. X. Wa, J. Y. Rong, and Y. Li, "Reduced-order extended state observer based event-triggered sliding mode control for DC-DC buck converter system with parameter perturbation," *Asian J. Control*, vol. 23, no. 3, pp. 1591–1601, 2021. http://doi.org/10.1002/asjc.2301

[18] Z. Karami, Q. Shafiee, S. Sahoo, M. Yaribeygi, H. Bevrani, and T. Dragicevic, "Hybrid model predictive control of DC-DC boost converters with constant power load," *IEEE Trans. Energy Convers.*, vol. 36, no. 2, pp. 1347–1356, 2021. http://doi.org/10.1109/tec.2020.3047754